INTERNATIONAL JOURNAL FOR NUMERICAL METHODS IN FLUIDS
Int. J. Numer. Meth. Fluids 2004; **44**:837–860 (DOI: 10.1002/fld.673)

Large eddy simulation (2D) using diffusion–velocity method and vortex-in-cell

R. E. Milane*,†

Department of Mechanical Engineering, University of Ottawa, Ottawa, Ont., Canada K1N 6N5

SUMMARY

A large eddy Simulation based on the diffusion-velocity method and the discrete vortex method is presented. The vorticity-based and eddy viscosity type subgrid scale model simulating the enstrophy transfer between the large and small scale appears as a convective term in the diffusion-velocity formulation. The methodology has been tested on a spatially growing mixing layer using the two-dimensional vortex-in-cell method and the Smagorinsky subgrid scale model. The effects on the vorticity contours, momemtum thickness, mean streamwise velocity profiles, root-mean-square velocity and vorticity fluctuations and negative cross-stream correlation are discussed. Comparison is made with experiment and numerical work where diffusion is simulated using random walk. Copyright © 2004 John Wiley & Sons, Ltd.

KEY WORDS: large eddy simulation; diffusion-velocity method; Smagorinsky subgrid scale model; vortex-in-cell; spatially growing mixing layer

1. INTRODUCTION

In recent works, the vortex method in a purely Lagrangian frame (particle representation) has been developed in the context of large eddy simulation (LES) using the eddy viscosity subgrid scale (SGS) model [1]. Both the Smagorinsky and dynamic eddy viscosity models were implemented and the constants were obtained specifically for the vorticity equation. In the particle representation, the eddy viscosity model was implemented by modifying the strength of the particles using the integral approximation for the solution of the diffusion equation [2], also denoted as the particle strength exchange (PSE). In other development, Milane and Nourazar [3] and Milane and Nourazar [4] used the core-spreading technique to simulate the diffusion equation in the context of a LES where the eddy viscosity SGS vorticity model [5] and the SGS turbulent kinetic energy model [6] were tested, respectively.

*Correspondence to: R. E. Milane, Department of Mechanical Engineering, University of Ottawa, 770 av. King Edward, Ottawa, Ont., Canada K1N 6N5.
†E-mail: milane@eng.uottawa.ca

Contract/grant sponsor: National Sciences and Engineering Research Council of Canada

Received 14 July 2003
Revised 5 November 2003

The core-spreading technique is valid in the limit of vanishing viscosity [7, 8]. Cottet [9] presented subgrid scale model based on a rigorous analysis of truncation error of the filtered vorticity equation. The author developed a scheme based on the PSE method for small scale contribution. The method was tested by removing all the backscatter produced by the flow strain.

The diffusion-velocity method is an alternative way for simulating the diffusion equation [10–14] and can be extended to an eddy viscosity based LES formulation. Originally, Ogami and Akamatsu [10] introduced the method as an alternative to the random walk solution of the diffusion equation in order the extend the solution to Reynolds number values below the lower limit of applicability of the random walk. The authors [10] argued that the diffusion-velocities being proportional to the negative of vorticity gradient and the kinematic viscosity yield a net flow of vorticity with a positive flux from a region of higher vorticity to a region of lower vorticity, consistent with the physics of diffusion. Recently, Beaudoin *et al*. [14], using the diffusion-velocity method as an alternative to PSE method, concluded that for anisotropic diffusion problems it is by far easier to derive than that of the PSE method.

The methodology that extends the diffusion-velocity method to a LES using an eddy viscosity SGS model and solves the vorticity equation using the vortex method has not yet been developed and tested. Therefore the objective of this study is to develop this methodology and to show that it can simulate the dissipative effect of a SGS model. In the context of a LES based on an eddy viscosity SGS model and on the vortex method, the importance and advantage of the diffusion-velocity method stems from the fact that the filtered vorticity equation has fewer types of terms in comparison with the alternative where the terms with the eddy viscosity are expanded as will be shown in Section 2.2.1. In vortex methods, the diffusion-velocity method [10–13] has so far been used in two-dimensional calculations. The encouraging previous results have motivated the present investigation which extends the diffusion-velocity method to a LES based on eddy viscosity SGS models. The success of the present study will warrant developing further the method to three-dimensional LES and DNS.

The feasibility of the method will be illustrated using the two-dimensional mixed Lagrangian-Eulerian vortex-in-cell (VIC) method applied to a spatially growing mixing layer and using the Smagorinsky SGS model. The two-dimensional mixing layer is selected because the trend in the flow characteristics, i.e. the vorticity contours, momemtum thickness, mean streamwise velocity profiles, root-mean-square velocity and vorticity fluctuations and negative cross-stream correlation have been previously obtained using the vortex method without SGS modelling [15–17]. Therefore these trends can be used as a base to compare the present results. Also the simulation of the 2D mixing layer using vortex method based on the diffusion-velocity method without SGS modelling has not yet been reported. Furthermore the VIC method is used because it combines the best features of Lagrangian and Eulerian methods, i.e. the numerical dissipation is reduced relative to the purely Eulerian method [18–21] and the computational time is reduced relative to the Lagrangian method. In the VIC method, Eulerian scheme is used to calculate the velocity field and a Lagrangian scheme to track the vortices. The vortices that represent fluid particles with concentrated vorticity (vortex points or blobs) are tagged and traced in time. As time proceeds, the change of vorticity distribution within a blob is governed by the vorticity transport equation. The justification for this method stems from the fact that, in turbulent flows, vorticity is often very large in thin threadlike fluid, while the remaining fluid is virtually without vorticity. Therefore, the vorticity can be lumped into concentrated vortex blobs around which the fluid spins. The computational results will be compared with

experimental results of Masutani and Bowman [22] because the two-dimensionality of the flow was carefully maintained and verified.

2. GOVERNING EQUATIONS

2.1. Vorticity equation

The continuity and vorticity transport equations for an incompressible and viscous fluid flow are, respectively,

$$\frac{\partial u_i}{\partial x_i} = 0 \tag{1}$$

$$\frac{\partial \omega_i}{\partial t} + u_j \frac{\partial \omega_i}{\partial x_j} = \omega_j \frac{\partial u_i}{\partial x_j} + \nu \frac{\partial^2 \omega_i}{\partial x_j \partial x_j} \tag{2}$$

where ω_i represents the component of the vorticity vector ω, u_i and u_j represent the components of the velocity vector $\mathbf{u}$, and ν is the kinematic viscosity. The left-hand side of Equation (2) includes the rate of change of vorticity in time and due to convection, respectively. The first term on the right-hand side is the vortex stretching term, and the second term on the right-hand side is the viscous diffusion.

For a 2D flow parallel to (x, y)-plane, the velocity vector is $\mathbf{u} = \mathbf{u}(x, y, t)$, the vorticity vector (ω_z) reduces to one component in the z-direction perpendicular to the (x, y)-plane, and the stretching term vanishes. Therefore Equation (2) reduces to

$$\frac{\partial \omega_z}{\partial t} + u_j \frac{\partial \omega_z}{\partial x_j} = \nu \frac{\partial^2 \omega_z}{\partial x_j \partial x_j} \tag{3}$$

A different form of vorticity equation can be written if the continuity (Equation (1)) is combined with the vorticity equation (Equation (3)) assuming constant viscosity as

$$\frac{\partial \omega_z}{\partial t} + \frac{\partial}{\partial x_j}\left\{u_j - \frac{\nu}{\omega_z}\frac{\partial \omega_z}{\partial x_j}\right\}\omega_z = 0 \tag{4}$$

Equation (4) is similar to the equation used by Ogami and Akamatsu [10] in the development of the diffusion-velocity method.

2.2. Filtered vorticity equation

For any time- and space-dependent variable $\phi(x, y, t)$, the spatial filtered value $\bar{\phi}$ is

$$\bar{\phi}(x, y, t) = \iint \phi(\zeta, \eta, t) G(x - \zeta, y - \eta)\, \mathrm{d}\zeta\, \mathrm{d}\eta \tag{5}$$

where $G(x, y)$ is the spatial filter shape. For a two-dimensional flow, the velocity and vorticity fields are decomposed in the filtered field (overline), and the subgrid-scale field (superscript) as

$$\omega_x = \omega_x'(x, y; t); \quad \omega_y = \omega_y'(x, y; t); \quad \omega_z = \bar{\omega}_z(x, y; t) + \omega_z'(x, y; t)$$

$$u = \bar{u}(x, y; t) + u'(x, y; t); \quad v = \bar{v}(x, y; t) + v'(x, y; t); \quad w = w'(x, y; t)$$

In the above decompositions, $\bar{w} = \bar{\omega}_x = \bar{\omega}_y = 0$ are needed for the 2-D formulation. The zero value for the filtered spanwise velocity, i.e. $\bar{w} = 0$, together with the zero value for the spanwise derivative of filtered quantities, i.e. $\partial(\bar{\ })/\partial z = 0$, are needed in the calculations of the modulus of the strain rate {Equation (16) in Section 2.2.2}. The zero values for $\bar{\omega}_x = \bar{\omega}_y = 0$ is a direct consequence of $\bar{w} = 0$ and $\partial(\bar{\ })/\partial z = 0$ in the definition of vorticity. In the two-dimensional calculations, it means that the initial spanwise vorticity ($\bar{\omega}_z$) in the whole domain remains in the spanwise direction throughout the simulation, therefore $\bar{\omega}_x = \bar{\omega}_y = 0$ throughout the simulation. The filtered vorticity components $\bar{\omega}_x$ and $\bar{\omega}_y$ appears in the model for the divergence of the SGS vorticity stress, i.e. Equation (13) in Section 2.2.1.

The filtered continuity equation obtained using Equation (1) and the filtered transport equation for the spanwise component $\bar{\omega}_z$ obtained using Equation (3) are (see for example Reference [1]), respectively,

$$\frac{\partial \bar{u}}{\partial x} + \frac{\partial \bar{v}}{\partial y} = 0 \tag{6}$$

$$\frac{\partial \bar{\omega}_z}{\partial t} + \bar{u}\frac{\partial \bar{\omega}_z}{\partial x} + \bar{v}\frac{\partial \bar{\omega}_z}{\partial y} = v\frac{\partial^2 \bar{\omega}_z}{\partial x^2} + v\frac{\partial^2 \bar{\omega}_z}{\partial y^2} - \frac{\partial Y}{\partial x} - \frac{\partial Z}{\partial y} \tag{7}$$

where the divergence of the SGS vorticity stress Y and Z responsible for the transfer of enstrophy between large and small scales are expressed as

$$\frac{\partial Y}{\partial x} = \frac{\partial}{\partial x}(\overline{u\omega_z} - \bar{u}\bar{\omega}_z - \overline{w\omega_x})$$

and

$$\frac{\partial Z}{\partial y} = \frac{\partial}{\partial y}(\overline{v\omega_z} - \bar{v}\bar{\omega}_z - \overline{w\omega_y}) \tag{8}$$

Another form for Equation (7) is obtained using the continuity [Equation (6)], rearranging the SGS and molecular diffusion terms as

$$\frac{\partial \bar{\omega}_z}{\partial t} + \frac{\partial\{\bar{u} + (Y/\bar{\omega}_z) - (v/\bar{\omega}_z)(\partial\bar{\omega}_z/\partial x)\}\bar{\omega}_z}{\partial x} + \frac{\partial\{\bar{v} + (Z/\bar{\omega}_z) - (v/\bar{\omega}_z)(\partial\bar{\omega}_z/\partial y)\}\bar{\omega}_z}{\partial y} = 0 \tag{9}$$

In Equation (9), the SGS and the molecular diffusion terms are treated as convective terms. This is similar to the procedure followed by Ogami and Akamatsu [10] in the development of the diffusion-velocity method (see Equation (4) also).

Another equation used in the VIC method is derived using the definition of vorticity vector,

$$\bar{\omega}_z = \frac{\partial \bar{v}}{\partial x} - \frac{\partial \bar{u}}{\partial y} \tag{10}$$

Since the divergence of the velocity is zero because of the continuity equation [Equation (6)], therefore the components of the velocity **u** can be expressed as the gradients of a scalar, i.e. gradients of the streamfunction ψ,

$$\bar{u} = \frac{\partial \psi}{\partial y}, \quad \bar{v} = -\frac{\partial \psi}{\partial x} \tag{11}$$

Combining Equations (10) and (11), Poisson's equation is obtained as

$$\nabla^2\psi = -\bar{\omega}_z \tag{12}$$

The solution of Poisson's equation is given by the Green's function or the Biot–Savart [23]. It is equivalent to the solution obtained by $\boldsymbol{u} = (\bar{u}, \bar{v})$ in the convective part of Equation (9).

2.2.1. Formulation with eddy viscosity based SGS Model. The two groups of terms Y and Z in Equation (7), describing the contribution of the small scales are the SGS vorticity stress. Their net effect is to transfer enstrophy from the large-scale to the small scale. By analogy with the SGS Reynolds stress in the filtered momentum, the SGS vorticity stress is modelled using the eddy viscosity concept in such a way that its divergence appearing in Equation (7) is expressed as [1]

$$\begin{aligned} -\frac{\partial Y}{\partial x} - \frac{\partial Z}{\partial y} = {} & \frac{\partial}{\partial x}\left\{ v_{Tx}\frac{\partial \bar{\omega}_z}{\partial x}\right\} + \frac{\partial}{\partial y}\left\{ v_{Ty}\frac{\partial \bar{\omega}_z}{\partial y}\right\} + \frac{\partial}{\partial z}\left\{ v_{Tz}\frac{\partial \bar{\omega}_z}{\partial z}\right\} \\ & - \frac{\partial v_{Tx}}{\partial x}\frac{\partial \bar{\omega}_x}{\partial z} - \frac{\partial v_{Ty}}{\partial y}\frac{\partial \bar{\omega}_y}{\partial z} - \frac{\partial v_{Tz}}{\partial z}\frac{\partial \bar{\omega}_z}{\partial z} \end{aligned} \tag{13}$$

In two-dimensional calculations the last four terms in Equation (13) are nil. Therefore, Equation (13) implies that for an anisotropic flow, $-Y = v_{Tx}\partial\bar{\omega}_z/\partial x$ and $-Z = v_{Ty}\partial\bar{\omega}_z/\partial y$ where v_{Tx} and v_{Ty} are eddy viscosities in x- and y-directions, respectively. Substituting for Y and Z in Equation (9) and rearranging

$$\frac{\partial \bar{\omega}_z}{\partial t} + \frac{\partial\{\bar{u} - (v + v_{Tx})/\bar{\omega}_z\,\partial\bar{\omega}_z/\partial x\}\bar{\omega}_z}{\partial x} + \frac{\partial\{\bar{v} - (v + v_{Ty})/\bar{\omega}_z\,\partial\bar{\omega}_z/\partial y\}\bar{\omega}_z}{\partial y} = 0 \tag{14}$$

The terms $\left(u_{\mathrm{d}} = -\frac{(v+v_T)}{\bar{\omega}_z}\frac{\partial\bar{\omega}_z}{\partial x}, v_{\mathrm{d}} = -\frac{(v+v_T)}{\bar{\omega}_z}\frac{\partial\bar{\omega}_z}{\partial y}\right)$ that are added to the convective velocity are the components of the diffusion-velocity governed by both molecular diffusion and eddy viscosity from SGS model. It is noted that the non-linearity of the diffusion term in LES is a consequence of the eddy viscosity in the SGS model which is related to the flow field rather than the diffusion-velocity method itself. In DNS application, the diffusion-velocity method yields a linear diffusion term.

As an alternative to Equation (14) which will result in a diffusion term that could be treated using the PSE scheme or other schemes, the two terms with SGS eddy viscosity on the LHS of Equation (14) can be expanded as

$$\begin{aligned} & \frac{\partial\{-(v + v_{Tx})/\bar{\omega}_z(\partial\bar{\omega}_z/\partial x)\}\bar{\omega}_z}{\partial x} + \frac{\partial\{-(v + v_{Ty})/\bar{\omega}_z(\partial\bar{\omega}_z/\partial y)\}\bar{\omega}_z}{\partial y} \\ & = -(v + v_{Tx})\frac{\partial^2\bar{\omega}_z}{\partial x^2} - (v + v_{Ty})\frac{\partial^2\bar{\omega}_z}{\partial y^2} - \frac{\partial v_{Tx}}{\partial x}\frac{\partial\bar{\omega}_z}{\partial x} - \frac{\partial v_{Ty}}{\partial y}\frac{\partial\bar{\omega}_z}{\partial y} \end{aligned} \tag{15}$$

The first two terms on the RHS corresponding to the second-order derivatives of vorticity could be solved using either one of the three methods, i.e. the PSE scheme or the core spreading technique or the random walk method. The performance of these methods in LES is left to future studies, keeping in mind that the core spreading technique is limited to

cases of vanishing viscosity [7, 8] and the random walk is limited to high Reynolds number flows [24]. Furthermore in the context of LES based on eddy viscosity SGS models and the vortex method, Equation (15) suggests that the diffusion-velocity method is advantageous because one type of terms on the LHS has to be solved rather than two types of terms on RHS, i.e. terms with second-order derivatives of vorticity and terms with product of first-order derivatives of eddy viscosity and vorticity.

2.2.2. Smagorinsky SGS model. The constant in SGS model is function of the type of governing equations (vorticity or momemtum) and of the SGS model used. A few works using the vorticity equation are available. Mansfield *et al.* [1] obtained the constant in the Smagorinsky SGS model by balancing enstrophy production and dissipation for homogeneous and isotropic flow. Therefore it has been adopted in this study. Furthermore the Smagorinsky SGS model has been extended to anisotropic flow [25, 26] as

$$\nu_{Tx} = C_{\mathrm{r}}^2(\Delta^3)^{2/9}\Delta_x^{4/3}(2S_{ij}S_{ij})^{1/2}$$

and

$$\nu_{Ty} = C_{\mathrm{r}}^2(\Delta^3)^{2/9}\Delta_y^{4/3}(2S_{ij}S_{ij})^{1/2} \tag{16}$$

where $S| \equiv (2S_{ij}S_{ij})^{1/2}$ is the modulus of the strain rate and the constant $C_{\mathrm{r}} = 0.12$. Equation (16) is an extension of Smagorinsky model developed for isotropic flow to anisotropic flow by simply using different filter sizes Δ_x and Δ_y, in x- and y-directions, respectively, $\Delta = (\Delta_x\Delta_y)^{1/2}$. The filter sizes are a multiple (>1) of grid sizes. The Smagorinsky subgrid model was used even though it is too dissipative (see for example Reference [27]) because the objective of this study is to show that the diffusion-velocity method can simulate the dissipative effect of a SGS model. If so, it is expected that any other eddy viscosity based SGS model (non-dynamic and dynamic) would behave qualitatively in the same fashion.

3. VORTEX-IN-CELL

The vorticity field is discretized into a set of vortex particles. The motion of the vortex particles is governed by the vorticity transport equation [Equation (14)]. The discretization of the field into vortex particles will be discussed in Section 3.1. In the vortex-in-cell method, the vorticity is transferred from the vortex particles to the nodes of a two-dimensional grid, using an interpolation technique. This step will be discussed in Section 3.2. The motion of the vortex particles is traced by splitting the vorticity transport equation into substeps. In the first substep, the convection of the interacting vortex particles is obtained by first calculating the components of the velocity $\boldsymbol{u} = (u, v)$ at the nodes by solving the Poisson's equation [Equation (12)]. Then the components of the diffusion-velocities are calculated at the nodes as $(-(\nu + \nu_T)/\bar{\omega}_z(\partial\bar{\omega}_z/\partial x), -(\nu + \nu_T)/\bar{\omega}_z(\partial\bar{\omega}_z/\partial y))$. The velocity components $\mathbf{u} = (u, v)$ at the nodes and the diffusion-velocities are transferred to the location of each vortex particle, using an interpolation technique. Then the vortex particles are convected using the equation of motion of a material point using a two-step viscous splitting algorithm. This step will be discussed in Section 3.3. No additional substep is needed for the velocity-diffusion method. However a second substep has been considered in this study in simulating the molecular

diffusion term without SGS model using random walk. In this case the diffusion-velocity term is replaced by the random walk. A comparison between the two methods is made in Section 6.3. Also a regridding procedure used to improve the accuracy of the calculations by inserting or removing vortex particles whenever the distance between two neighbouring vortex blobs is outside a range specified by a criteria was implemented [28]. The procedure was tested on runs without SGS model. The effect on the mixing layer flow characteristics were small probably because the number of vortex particles used was high. Therefore the regridding procedure was not used in the runs presented in this study in order to reduce the computational time.

3.1. Vortex particles

In vortex methods, the vorticity field is discretized into N_p point vortices, each with circulation Γ_i, and the vorticity field is given as

$$\omega(x) = \sum_{i=1}^{N_p} \Gamma_i \delta(x - x_i) \tag{17}$$

where $\delta(x)$ is the Dirac delta function, $\boldsymbol{x}$ represents the co-ordinates at which vorticity is calculated and x_i is the co-ordinates position of the vortex points. The point vortices are vortex blobs rather than vortex points because the Biot–Savard law, i.e. the Green's function, has a singularity at the origin. It creates large velocities in its neighbourhood, which causes numerical as well as theoretical instabilities. To remove this difficulty, finite core size vortices or blob vortices may be used instead of point vortices [24]. Thus inside the core, velocity is smooth and is finite at the centre of the core. Although this trick creates some errors, it is very effective in removing the singularities from the flow field. By using this technique the velocity field induced by each vortex is quantitatively correct, only away from the centre of the vortices. In the vortex blob approach, the particles have a core radius σ (in VIC σ is equal the grid size), a volume δv_i and a vorticity vector of magnitude ω_i smoothened within the volume δv_i. For a given vortex particle, the circulation Γ_i is identical to the product of the vorticity and the volume of the vortex particle, $\omega_i \delta v_i$, which also represents the contribution of the vortex particle to the vorticity field. Therefore each vortex particles, is completely characterized by $(\boldsymbol{x}, \Gamma_i)$ and the vorticity field is given as

$$\omega(x) = \sum_{i=1}^{N_p} \Gamma_i \zeta_\sigma(\boldsymbol{x} - \boldsymbol{x}_i) \tag{18}$$

where the smoothing function $\zeta_\omega(\boldsymbol{x} - \boldsymbol{x}_i)$ is expressed as

$$\zeta_\sigma(\boldsymbol{x} - \boldsymbol{x}_i) = \frac{1}{\sigma^2} \zeta\left(\frac{\boldsymbol{x} - \boldsymbol{x}_i}{\sigma}\right) \tag{19}$$

with $\int \zeta(x)\,\mathrm{d}x = 1$. For the present 2D formulation, the vorticity field is given as

$$\omega(x) = \frac{1}{\sigma^2} \sum_{i=1}^{N_p} \Gamma_i \zeta\left(\frac{x - x_i}{\sigma}\right) \zeta\left(\frac{y - y_i}{\sigma}\right) \tag{20}$$

where $[(x - x_i)/\sigma, (y - y_i)/\sigma]$ are the co-ordinates distance in units of core size.

3.2. Interpolation scheme

The smoothing functions used are the area-weighing scheme [29],

$$\zeta(\eta) = (1 - |\eta|), \quad |\eta| < 1 \tag{21a}$$

and the M_4' scheme, a higher order scheme [8],

$$\zeta(\eta) = \begin{cases} 1 - \dfrac{5}{2}|\eta|^2 + \dfrac{3}{2}|\eta|^3, & |\eta| < 1 \\ \dfrac{1}{2}(2 - |\eta|)^2(1 - |\eta|), & 1 < |\eta| < 2 \\ 0, & |\eta| > 2 \end{cases} \tag{21b}$$

Results obtained from the two schemes will be compared in Section 6.2. The interpolation scheme [Equations (20) and (21a–b)] is used to transfer the vorticity from the vortex blobs to the nodes of the grid. A vortex blob contributes to the nearest 4 nodes and 16 nodes for the area-weighing scheme and the M_4' scheme, respectively. The total vorticity at each node is obtained by summing the vorticity contributions of all the vortex particles which are within one grid or two grids from that node for the area-weighing scheme and the M_4' scheme, respectively. Also since there are at least one vortex blob per grid, therefore the vortex blobs will always overlap. The position vector of the vortex blob centre is determined by (x_i, y_i) and is discussed in the next section.

3.3. First substep

The Poisson's equation, (Equation (12)), is solved in order to obtain the velocity components at each node, using the successive-over-relaxation method with central difference approximation for the derivatives [15], also called the extrapolated Liebmann's method. Once the components of the velocity at the nodes $\boldsymbol{u}_n = (u_n, v_n)$ are calculated, the components of the velocity $\boldsymbol{u}_i = (u_i, v_i)$ acting on the centre of the vortex blob, is calculated using the interpolation technique as

$$u_i = \sum_n u_n \zeta\left(\frac{x_i - x_n}{\sigma}\right) \zeta\left(\frac{y_i - y_n}{\sigma}\right) \tag{22a}$$

$$v_i = \sum_n v_n \zeta\left(\frac{x_i - x_n}{\sigma}\right) \zeta\left(\frac{y_i - y_n}{\sigma}\right) \tag{22b}$$

where n is representative of the nearest 4 nodes or 16 nodes surrounding the vortex blob in the area-weighing scheme or the M_4' scheme, respectively. The position vector of the vortex blob centre $\chi = (x_i, y_i)$ is calculated by integrating the equation of motion of a material point

$$\mathrm{d}\chi/\mathrm{d}t = \mathbf{u}(\chi(x, y, z, t)) \tag{23}$$

using the improved Euler's method where the predictor is

$$\chi^*(t + \Delta t) = \chi(t) + \mathbf{u}\Delta t \tag{24a}$$

and the corrector is

$$\chi(t + \Delta t) = \chi(t) + (\mathbf{u} + \mathbf{u}^*)\Delta t/2 \tag{24b}$$

Δt is the time-step and the velocity $\mathbf{u} = \boldsymbol{u}_i$. To implement Equations (24a) and (24b), the calculations are carried out in two steps within each time step. In the first step, the algorithm is executed using the predictor, Equation (24a). At the end of this step, the values are denoted by the superscript (*). Then, the algorithm is repeated using the corrector, Equation (24b). Two values of each variables are stored at each time-step, i.e. the old value at time t and the predicted value denoted by (*). At the end of the calculations, the old value is replaced by an updated value at time $t + \Delta t$.

After completing the above operation, the components of the diffusion-velocities are calculated at the nodes, $(u_{\mathrm{d}i} = -(v+v_T)/\bar{\omega}_z \partial\bar{\omega}_z/\partial x, v_{\mathrm{d}i} = -(v+v_T)/\bar{\omega}_z \partial\bar{\omega}_z/\partial y)$, and transferred to the centre of the vortex blob using Equations (22a) and (22b) and the position vector of the vortex blob is calculated using Equations (24a) and (24b) in which $\mathbf{u} = \boldsymbol{u}_{\mathrm{d}i}$. The diffusion-velocity could be unreasonably high in regions of small vorticity and non-zero vorticity gradient because it is inversely proportional to the vorticity. This problem is remedied by setting the components of the diffusion-velocity to zero whenever the vorticity at the nodes is less than 0.1% of the vorticity associated with vortex particle.

Here it is noted that the solution of the Poisson's equations together with the Lagrangian movement of the vortex particles is equivalent to the solution of the convective term $\boldsymbol{u} = (\bar{u}, \bar{v})$ in Equation (14).

3.4. Second substep: random walk

For the case without SGS model, the diffusion term in Equation (7) is

$$v\left(\frac{\partial^2\bar{\omega}_z}{\partial x^2} + \frac{\partial^2\bar{\omega}_z}{\partial y^2}\right)$$

This term can be simulated using random walk for high Reynolds number [24]. This is handled by superimposing on the motion due to the convection of the vortices from the first substep (without the contribution of the diffusion-velocity), the random walk using first the predictor Equation (24a) as

$$\chi^*(t + \Delta t) = \chi(t) + \boldsymbol{u}\Delta t + \eta_1 \tag{25a}$$

then the corrector (Equation (24b)) as

$$\chi(t + \Delta t) = \chi(t) + (\boldsymbol{u} + \boldsymbol{u}^*)\Delta t/2 + \eta_2 \tag{25b}$$

where $\mathbf{u} = \boldsymbol{u}_i, \eta_1$ and η_2 are obtained from a Gaussian distribution with zero mean and standard deviation $(2v\Delta t)^{1/2}$.

4. BOUNDARY AND INITIAL CONDITIONS

The computational domain in Figure 1 consists of a rectangular grid with uniform grid size in each direction and in general $(\delta_x \neq \delta_y)$. The lower left corner of the grid is located at $x = 1$ and $y = 1$. The boundary conditions for LES are the same as for the unfiltered case because they are assumed to be governed by the large scale. The Neumann conditions apply to the

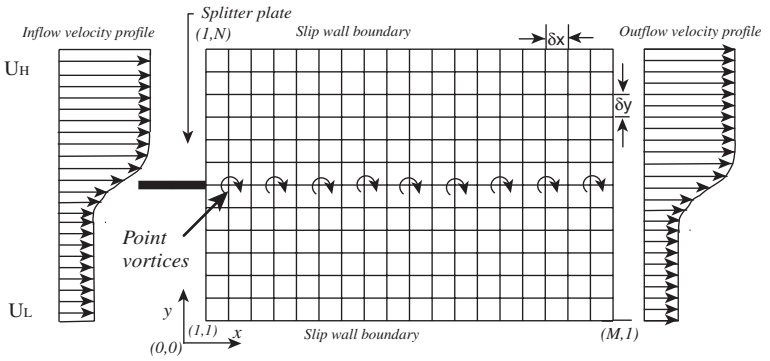

Figure 1. Computational domain, rectangular grid, initial position of the vortices, and boundary conditions.

inflow and outflow boundaries with $\psi = 0$ at $y = 0$. The inflow and outflow streamfunction profiles correspond to profiles of velocity that are error functions in such a way that

$$(\partial\psi/\partial y)_{N,j} = (\Delta U/2)\,\mathrm{erf}\{\sigma(y - y_{\mathrm{ov}})/(x - x_{\mathrm{v}})\} + U_{\mathrm{c}} \tag{26}$$

where subscript $N = 1$ and M correspond to the node in the x-direction at inflow and outflow, respectively, j corresponds to the node in the y-direction, $\Delta U = U_{\mathrm{H}} - U_{\mathrm{L}}$ is the velocity difference across the layer, U_{H} and U_{L} are the velocities of the high-speed side and the low-speed side, respectively, y_{ov} is the ordinate of the centreline, x_{v} is the virtual origin, σ is the spreading parameter and $U_{\mathrm{c}} = (U_{\mathrm{H}} + U_{\mathrm{L}})/2$ is the average velocity. In addition in order to simulate the Kelvin–Helmholtz instability mechanism, the profile may be augmented by a perturbation based on linear stability analysis [30]. Another approach that does not rely on stability analysis may be used as discussed in Inoue [16]. In vortex method, the Kelvin–Helmholtz instability may be simulated by moving vertically the vortex closest to the edge of the splitter plate by a small distance (perturbation) given by a sinusoidal function of time operating at the fundamental frequency (f) of the unforced mixing layer as

$$y(t) = Ax\,\sin(2\pi f t) \tag{27}$$

where $A = 0.5U_{\mathrm{c}}\Delta t$ is the amplitude and x represents a small percentage of A ($x = 3.0\%$ in this study). The fundamental frequency f is calculated using $f\theta_i/(2U_{\mathrm{c}}) \approx 0.02$ [31] where θ_i is the momentum thickness at the beginning of the region of linear growth. The factor A has been used by Inoue [16] where a forced mixing layer was investigated. In this study the small value of $x = 3.0\%$ introduced ensures that the mixing layer is in the unforced mode.

Also rather than specifying an error function as the outflow boundary condition, i.e. Equation (26), the convective outflow boundary condition was considered. Comparison of the results of momemtum thickness obtained using Equation (26) at outflow with the ones obtained using the convective outflow boundary condition, i.e. without Equation (26), showed no significant difference up to $x/H \approx 0.25$ cm, after which the momentum thickness growth rate is faster without Equation (26). The error function outflow boundary condition has been adopted because it constrains the growth rate of the momentum thickness, and yields a slope for the linear growth region in close agreement with the experiment [15].

Furthermore, slip conditions are assumed for the top and bottom boundaries. The Dirichlet condition is used for the bottom boundary at $y_L = 1$, consistent with $\psi_{i,0} = 0$ at $y = 0$, as

$$\psi_{i,1} = y_L U_L \tag{28}$$

and for the top boundary

$$\psi_{i,N} = U_L y_{sp} + U_H(y_{i,N} - y_{sp}) \tag{29}$$

where y_{sp} is the splitter plate y location and N corresponds to the nodes at the top boundary.

Initially, the velocity discontinuity across the splitter plate is simulated using a vortex sheet, discretized into a row of point vortices as shown in Figure 1. At time $t = 0$, the point vortices are equidistant, and separated by a distance $d = H/N_v$, where N_v is the number of vortices and $H = \delta_x M$ is the computational domain length. The vortex closest to the edge of the splitter plate is moved vertically using Equation (27) to initialize the Helmholtz instability. The unfiltered total circulation in the computational domain is $H(U_H - U_L)$. The circulation is equally distributed among the N_v vortices as $\Gamma_i = H(U_H - U_L)/N_v = d(U_H - U_L)$. Furthermore, if at the end of each time step Δt, defined as the characteristic time $\Delta t = d/U_c$, a vortex with circulation Γ_i is introduced at the trailing edge of the splitter plate, the vorticity generation rate is $\Gamma_i/\Delta t = (U_H - U_L)U_c$ and therefore the Kutta condition is satisfied. The oldest vortex, i.e. the vortex with the largest residence time, is discarded from the calculations when a new vortex is introduced at the edge of the splitter plate. Furthermore, the vortices can move freely in and out through the outflow boundary to avoid the collection of vortices at the end of the computational domain. The motion of the vortices outside the computational domain is assumed to be governed by the velocity at the outflow boundary.

In the LES, the initial circulation of the vortices should be filtered. However approximating the vorticity field using Equation (20) corresponds to filtering the circulation of each vortex Γ_i using the smoothing function $\zeta(\boldsymbol{x} - \boldsymbol{x}_i)$ [1, 9]. As noted earlier, in vortex method, smoothing or filtering has been used in order to remove the singularity in Biot–Savard law. Therefore the vorticity field given by Equation (20) is interpreted as the filtered vorticity field used in LES. Two questions remain to be addressed, the correspondence between the smoothing function and the LES filter shape and between the core size used in the smoothing function and the filter size Δ. Regarding the former issue, it is noted that for the Smagorinsky model no filter shape is invoked explicitly, therefore the smoothing function could be any of the ones used in VIC, such as area-weighing scheme or the M_4' scheme. Regarding the latter issue, the filter size is proportional to the core size since both are proportional to the grid size (the core size = grid size in VIC).

5. SOLUTION PROCEDURE FOR DIFFUSION-VELOCITY METHOD

The solution procedure to solve the velocity and vorticity fields consists in the following steps:

(a) Initializing by placing the equidistant vortices at the level of the splitter plate and by assuming arbitrary values for ψ at the internal nodes together with the boundary conditions [Equations (26)–(29)].

(b) Distributing the vorticity from the vortex particles to the nodes using the interpolation scheme [Equations (20) and (21a–b)].
(c) Solving the Poisson's equation [Equation (12)], using a Gauss–Seidel iteration with a left-to-right sweep of the nodes and bottom-to-top sweep of the lines. Iteration convergence is obtained when the percent difference between consecutive ψ is less than 0.001%.
(d) Computing the velocities u and v at the nodes using Equation (11).
(e) Calculating the velocities at the location of each vortex (u_n, v_n) using the interpolation scheme [Equations (22a–b)].
(f) Updating the co-ordinates of the vortices using Equations (24a–b).
(g) Computing the SGS eddy viscosity using Equation (16).
(h) Computing the diffusion-velocity at the nodes $(-(\nu + \nu_T)/\bar{\omega}_z \partial\bar{\omega}_z/\partial x, -(\nu + \nu_T)/\bar{\omega}_z \partial\bar{\omega}_z/\partial y)$.
(i) Calculating the diffusion-velocity at the location of each vortex using the interpolation scheme [Equations (22a–b)] where (u_n, v_n) are replaced by $(-(\nu + \nu_T)/\bar{\omega}_z \partial\bar{\omega}_z/\partial x, -(\nu + \nu_T)/\bar{\omega}_z \partial\bar{\omega}_z/\partial y)$.
(j) Updating the co-ordinates of the vortices using Equations (24a–b).
(k) Introducing a new vortex at the edge of the splitter plate, and discarding the oldest one.
(l) Marching in time by repeating the calculations from step b to k.

The first and second derivatives are calculated using fourth-order central difference formulas.

6. FLOW FIELD RESULTS

Several numerical experiments were conducted to validate the method. The diffusion-velocity method simulating molecular diffusion without SGS model, in conjunction with the vortex-in-cell method has not yet been presented in previous literature. Therefore the method will be first validated by comparing with the experimental mixing layer data of Masutani and Bowman [22] (MB), because the two-dimensionality of the flow was carefully maintained and verified, and also by comparing with a numerical experiment where molecular diffusion is simulated using random walk. Results obtained using the area-weighing scheme and the M_4' scheme are compared. Then LES results based on the diffusion-velocity method and the Smagorinsky subgrid scale model were obtained. Several flow characteristics are reported and compared, vorticity contours, mean velocity profiles, root-mean-square (rms) longitudinal and lateral velocity fluctuations, Reynolds shear stress, and rms vorticity fluctuations.

6.1. Flow and numerical parameters

The velocity ratio is $r = U_L/U_H = 0.5$ (ratio of the lower velocity side of the splitter plate to the higher velocity side) with the free stream velocity above the splitter plate $U_H = 600\,\text{cm/s}$ and below the splitter plate $U_L = 300\,\text{cm/s}$, similar to the parameters used in the experiment of MB. The spreading rate is $\sigma = 35$ for $r = 0.5$ [32]. The ordinate $y_{sp} = 33\,\text{cm}$ corresponds to the edge of the splitter plate in Figure 1. For the boundary condition [Equation (26)], the ordinate $y_{ov} = y_{sp}$ at inflow and $y_{ov} = 32\,\text{cm}$ at outflow. The reported results are for a viscous flow condition with $\nu = 14.5 \times 10^{-2}\,\text{cm}^2/\text{s}$ (the kinematic viscosity of air at 18°C).

The computational domain for the base run consists in a 256×256 anisotropic grid with equidistant grid, $\delta_x = 0.5$ cm and $\delta_y = 0.25$ cm. The aspect ratio $a_{xy} = \delta_x/\delta_y = 2.0$ is consistent with $a_{xy} = 2.0$ used by Deardoff [33] and $a_{xy} = 3.7$ used by Shumann [34] in LES of channel flow. Also Kaltenbach [35] has reported that the representation of shear flows is most economical when anisotropic grid (i.e. $a_{xy} > 1$) is used because it produces adequate values for ratios of Reynolds stresses. Also a numerical experiment using an isotropic grid, $\delta_x = \delta_y = 0.25$ cm with 512×256 grid, and using the same computational domain size as the base run, is reported. The area-weighting scheme was used in the base run. For all LES, the filter sizes are set to twice the grid size in each direction, i.e. $\Delta_x = 2\delta_x$ and $\Delta_y = 2\delta_y$.

At the level of the splitter plate, the shear layer is discretized into a layer of $N_v = 10\,240$ equidistant vortex particles. Therefore, the circulation of each vortex is $\Gamma_i = 37.5 \times 10^{-5}$ m^2/s, and the time step $\Delta t = d/U_c = 27.7 \times 10^{-6}$ s. $N_v = 10\,240$ means that there are 40 vortices $(40 = 10\,240/256)$ in one grid. Sensitivity of the results to the number of vortices was tested on the base run using $N_v = 2560$, i.e. 10 vortices per grid. No significant difference between $N_v = 10\,240$ and $N_v = 2560$ was found. In this study, the number of vortices is $N_v = 10\,240$ for all the reported runs.

The flow is allowed to develop for two residence times (i.e. $2M$ time-steps) before the statistical calculations are started. Then the mean flow is obtained using time-averaging over the next nine residence times, and the rms velocity fluctuations, the negative cross-stream correlation and the rms vorticity fluctuations are calculated using time-averaging over the next twenty five residence time. The numerical experiments are conducted on a DEC Alpha.

6.2. *Diffusion-velocity method without SGS*

The streamwise mean velocity normalized as $(U - U_L)/(U_H - U_L)$ is shown in Figure 2(a) as a function of the similarity variable $\eta_v = (y - y_0)/(x - x_v)$ at four downstream locations, where U is the streamwise mean velocity, y_0 is the ordinate of the velocity centreline at location x, the virtual origin defined as the x-location at the intersection of the velocity centreline with the horizontal line at the level of the splitter plate is 4.01 cm for all the runs with the diffusion-velocity method. Figure 2(a) shows that the agreement with the experiment of MB [22] (dark symbols) is adequate. The results of the numerical simulation are presented in the self-preserving region, which is from $x = 20$–70 cm, i.e. $0.16 < x/H < 0.6$. The self-preserving region corresponds to the region of linear growth of the momemtum thickness. Figure 9(b) shows the momentum thickness θ as a function of x/H for several cases. For the case without SGS (symbol $\triangle$), a region with a nearly linear growth is identified between $0.16 < x/H < 0.6$, where the slope is equal to about 0.0155. This value is close to the experimental value 0.0165 of MB.

The rms longitudinal (rmsu') and lateral (rmsv') velocity fluctuations normalized with ΔU are shown in Figures 2(b) and 2(c), respectively, and the Reynolds shear stress $(\overline{-u'v'})$ normalized with ΔU^2 is shown in Figure 2(d). Self-preserving profiles are obtained for $0.16 \leqslant x/H \leqslant 0.6$. The rmsu' is shown together with the data from the MB. The values for the rmsu' in the simulation slightly increase along the streamwise direction whereas it decreases in the experimental data. Similar behaviour is found in the numerical work of Ghoniem and Heidarinejad [17], who argued that the experimental trend is caused by dissipation due to molecular diffusion. The rmsv' is consistent with previous 2D simulation [15–17]. The data for $(\overline{-u'v'})/\Delta U^2$ are not reported in MB. However the peak values $(\overline{-u'v'})/\Delta U^2 = 0.012$ in

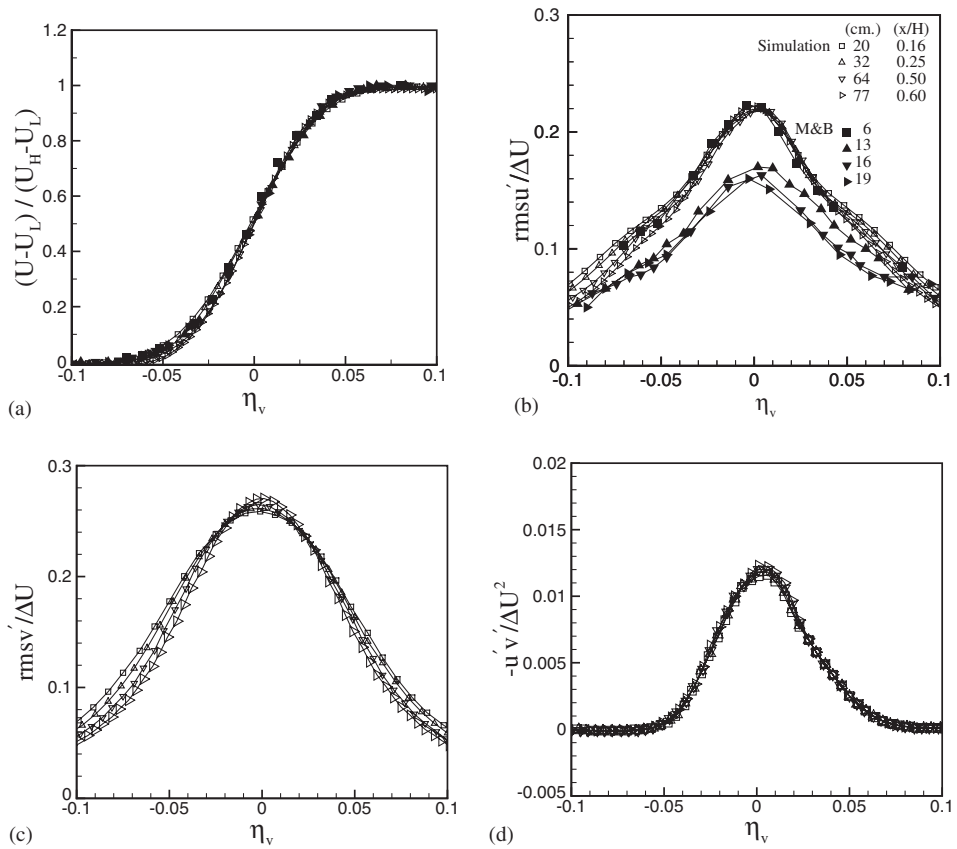

Figure 2. Normalized profiles at four downstream locations for case without SGS: (a) mean streamwise velocity, (b) rms longitudinal velocity fluctuations, (c) rms lateral velocity flucations, (d) negative cross-stream correlation. The mesh lines connecting the open symbols show the predicted profiles; the dark symbols correspond to the data from the experiment of MB.

Figure 2(d) is comparable with the peak of 0.013 obtained in the experiment of Oster and Wygnanski [31] for a velocity ratio of $r = 0.6$, which is slightly different than the value of $r = 0.5$ used in the present simulation.

Furthermore it is necessary to verify the sensitivity of the results to aspect ratio because results from LES are function of aspect ratios [35], particularly if they exhibit inhomogeneities of mean quantities as the mixing layer considered in this study where $\mathrm{rmsu}'/\mathrm{rmsv}' \approx 0.82$. Figures 3(a)–3(d) show that $\mathrm{rmsu}'/\Delta U, \mathrm{rmsv}'/\Delta U, -u'v'/\Delta U^2$, and $\mathrm{rms}\omega'$, respectively, are quite insensitive to aspect ratios tested. The rms vorticity fluctuations ($\mathrm{rms}\omega'$) has been reported in Figure 3(d) because the effect of LES on this quantity will be discussed in Section 6.5.

Figures 4(a)–4(d) show the $\mathrm{rmsu}'/\Delta U, \mathrm{rmsv}'/\Delta U, -u'v'/\Delta U^2$, and $\mathrm{rms}\omega'$ profiles for both the area-weighting scheme and the M_4' scheme. The peak of the $\mathrm{rmsu}'/\Delta U$ is slightly lowered when the M_4' scheme is used, whereas the peak of the $-u'v'/\Delta U^2$ is slightly higher as shown in Figures 6(b) and 6(d), respectively. The agreement between the profiles of the two schemes for the mean in Figure 6(a) and $\mathrm{rmsv}'/\Delta U$ in Figure 6(c) is closer than $\mathrm{rmsu}'/\Delta U$

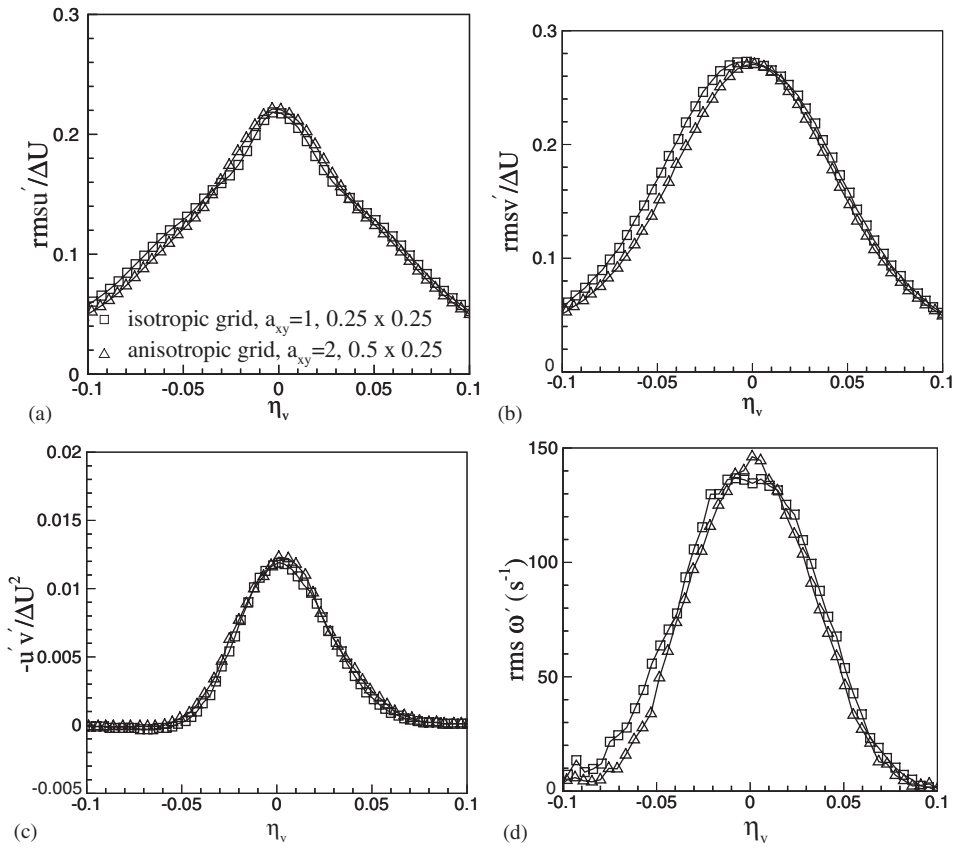

Figure 3. Sensitivity to aspect ratios (a) rms longitudinal velocity fluctuations, (b) rms lateral velocity fluctuations, (c) negative cross-stream correlation, and (d) rms velocity fluctuations for case without SGS at $x/H = 0.6$.

and $-u'v'/\Delta U^2$ profiles. However the figures suggest that the sensitivity of the profiles to the smoothing function is quite small probably because the number of vortex particles used is high. Therefore the M_4' scheme was not used in evaluating the diffusion-velocity method with SGS model in the interest of reducing the computational time. The computational time is reduced by about 10% when the area-weighting scheme is used in comparison with the M_4' scheme. The test using the M_4' scheme was conducted with a view that a better representation of vorticity on the nodes would improve the calculations of the diffusion-velocity. However from a practical point of view and for the mixing layer tested, the area-weighting scheme is adequate for the qualitative assessment of the diffusion-velocity method and will be used in remaining numerical experiments.

6.3. Comparison of diffusion-velocity method with random walk

The results of the diffusion-velocity method simulating the diffusion term is further validated by comparing with the results obtained using random walk. The virtual origin $x_v = 2.55$ cm

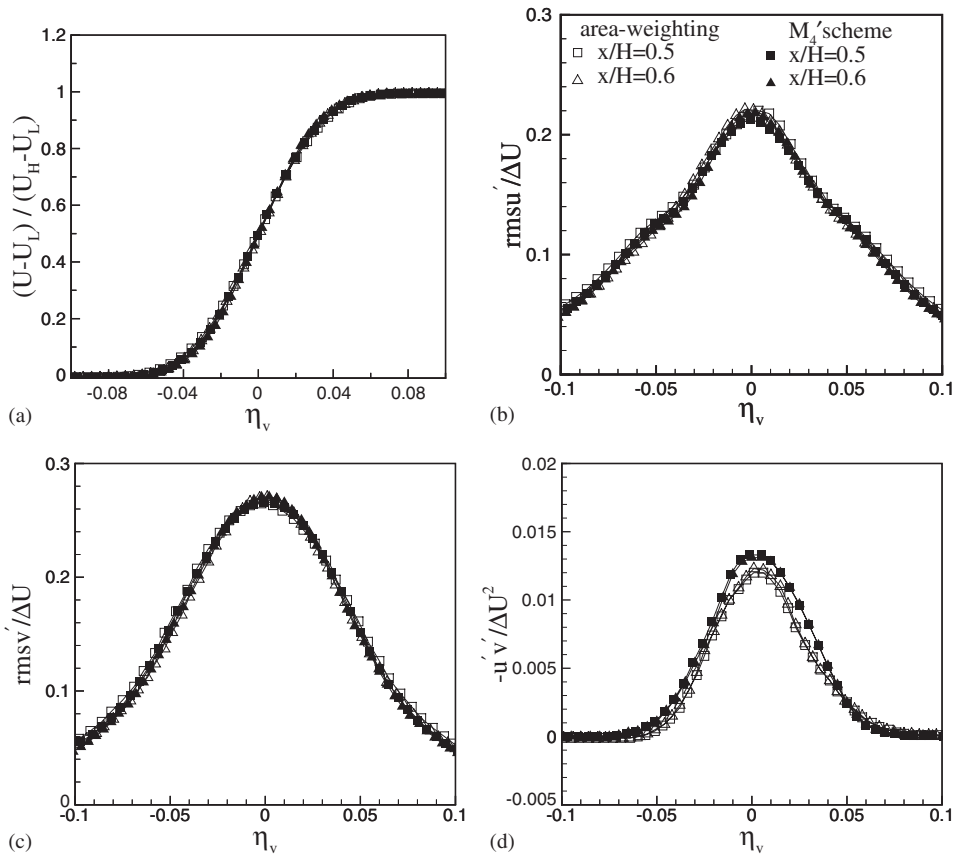

Figure 4. Comparison of are weighting scheme with M_4' scheme using diffusion velocity method without SGS model at two downstream locations; (a) streamwise mean velocity, (b) rms longitudinal velocity fluctuations, (c) rms lateral velocity fluctuations; (d) negative cross-stream correlation. Dark symbols, M_4' scheme; open symbols, area-weighting scheme.

when random walk is used. Figures 5(a)–5(d) show $(U - U_L)/(U_H - U_L)$, $\mathrm{rmsu}'/\Delta U, \mathrm{rmsv}'/\Delta U$, and $-u'v'/\Delta U^2$, respectively, at two downstream locations, $x/H = 0.5$ and 0.6. The difference in profiles due to the different methods is quite small. This difference is attributed to the different numerical errors in the two methods. No further elaboration is made in this study. The agreement between the profiles of the two methods provides further validation that the diffusion-velocity method is adequate.

6.4. LES run

Figures 6(a)–6(d) show $(U - U_L)/(U_H - U_L), \mathrm{rmsu}'/\Delta U, \mathrm{rmsv}'/\Delta U$, and $-u'v'/\Delta U^2$, respectively, for LES with Smagorinsky SGS model and $C_r = 0.12$. The mean in Figure 6(a) indicates adequate self-similar profiles at four downstream locations between $0.16 < x/H < 0.6$. This is consistent with nearly linear development of momemtum thickness in Figure 9(b) (symbol □).

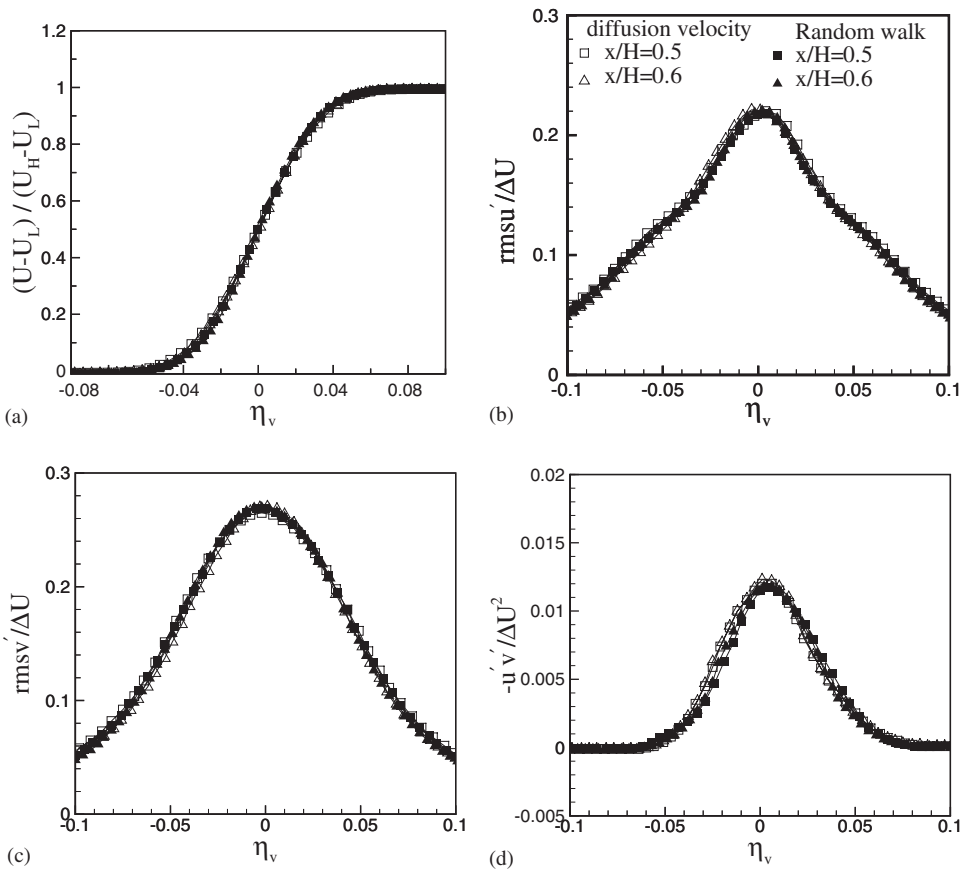

Figure 5. Comparison of diffusion velocity method with random walk at two downstream locations; (a) streamwise mean velocity, (b) rms longitudinal velocity fluctuations, (c) rms lateral velocity fluctuations; (d) negative cross-stream correlation. Dark symbols, random walk; open symbols, diffusion velocity method.

The $\mathrm{rmsu}'/\Delta U, \mathrm{rmsv}'/\Delta U$, and $-u'v'/\Delta U^2$ also show adequate similarity. However, the Reynolds shear stress $-u'v'/\Delta U^2$ in Figure 6(d) shows better similarity, similar to the mean in Figure 6(a). This is compatible with the fact that $-u'v'$ is linked to the mean flow by the mean momemtum equation and the self-similarity of the mean in Figure 6(a) is as good as $-u'v'/\Delta U^2$. It is noted that the profiles in Figures 6(a)–6(d) are not fully self-similar. This is consistent with the investigation of [27], who conducted LES based on the filtered Navier–Stokes equations and where tests using six non-dynamic and dynamic SGS models showed that the profiles are not fully self-similar.

6.5. *Comparison of LES runs with run without SGS*

Comparison between four runs is made: without SGS, Smagorinsky SGS using $C_r = 0.12$, Smagorinsky SGS using $C_r = 0.18$, and Smagorinsky SGS with $C_r = 0.12$ using an isotropic

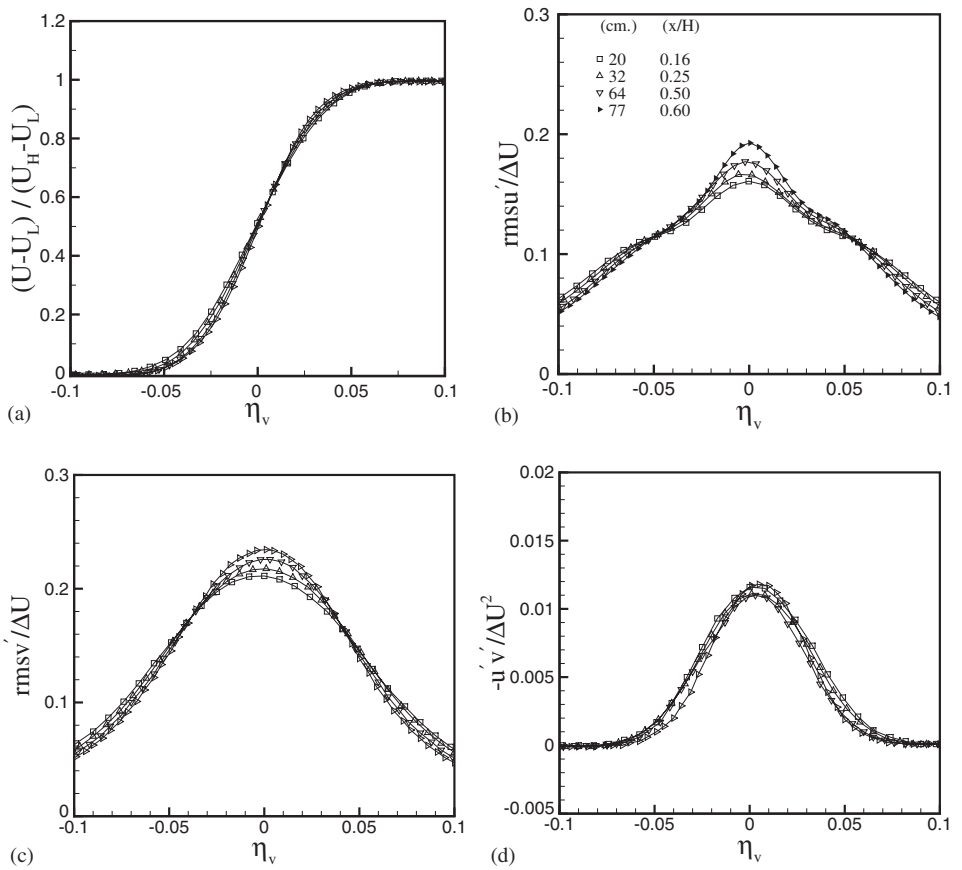

Figure 6. Normalized velocity profiles at four downstream locations for case with Smagorinsky SGS ($C_r = 0.12$): (a) streamwise mean velocity, (b) rms longitudinal velocity fluctuations, (c) rms lateral velocity fluctuations, (d) negative cross-stream correlation.

grid. The first three runs are conducted on an anisotropic grid. The case with Smagorinsky SGS using $C_r = 0.18$ is more dissipative than the case with $C_r = 0.12$ and therefore was chosen to verify whether the diffusion-velocity method predict the dissipative effect of SGS model. The isotropic case has finer grid in the x-direction only and generates a lower eddy viscosity from SGS model. It is compared with the anisotropic case, with a view to verify whether a lower eddy viscosity leads to less dissipation and therefore validate further the dissipative nature of the diffusion-velocity method when used in conjunction with a SGS model. Figures 7(a)–7(c) show the downstream evolution of the spanwise vorticity contours for the three cases with same anisotropic grid. The contours spread in the free stream as they develop from the edge of the splitter plate. The maximum contour level decreases as SGS model is applied consistent with its dissipative nature (see legend). It is 1800 for the case without SGS in Figure 7(a), 1500 for the case with Smagorinsky using $C_r = 0.12$ in Figure 7(b), and 1200 using $C_r = 0.18$ in Figure 7(c). Close up of selected downstream location are shown in Figures 8(a)–8(c) which are drawn using identical scale. Figure 8(a) without SGS indicates that the contour

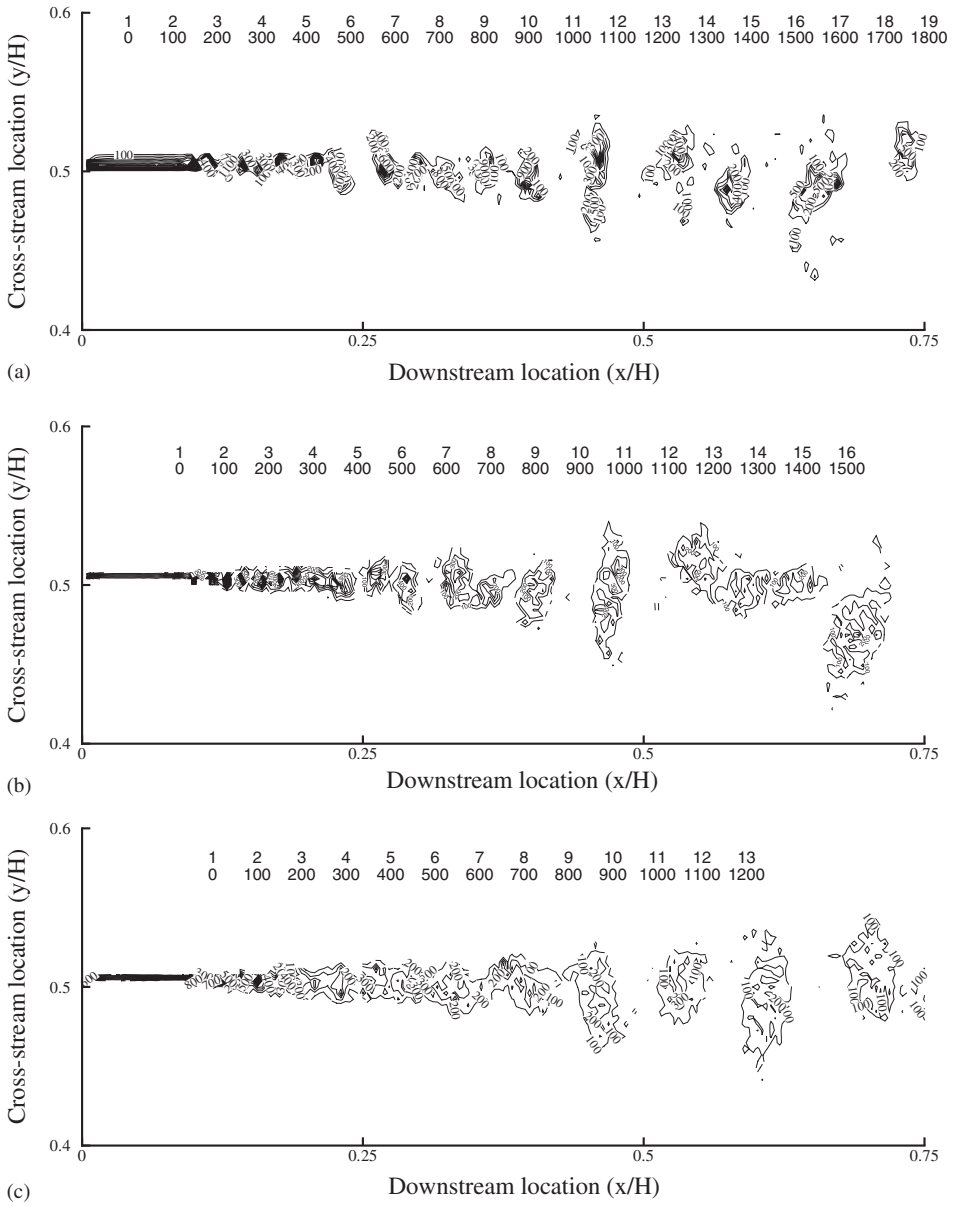

Figure 7. Vorticity contours for cases (a) without SGS, (b) with Smagorinsky SGS using $C_r = 0.12$, (c) with Smagorinsky SGS using $C_r = 0.18$. Contour level increment is 100.

peaks at 800, whereas it drops to 400 and 200 when the SGS with $C_r = 0.12$ and 0.18 are used, respectively. The contour levels are further apart when SGS model is used. Therefore, in the context of the diffusion-velocity method, the SGS model is dissipative because it decreases the contour peaks and yields coarser contour lines.

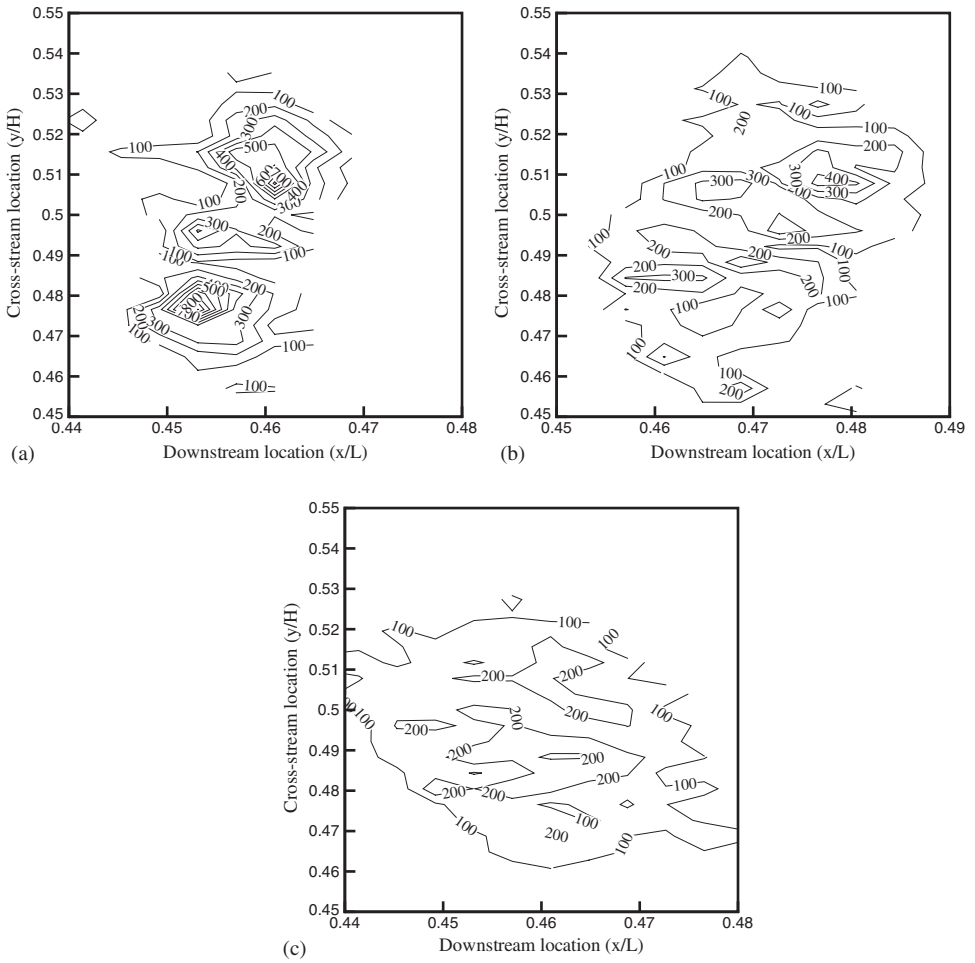

Figure 8. Vorticity contours at selected downstream location for cases (a) without SGS, (b) Smagorinky SGS ($C_r = 0.12$); (c) Smagorinsky SGS ($C_r = 0.18$). Contours level increment is 100.

The profiles of the various statistics are shown in Figures 9(a) and 10(a)–10(d) at downstream location $x/H = 0.6$ for the three cases discussed in the previous paragraph and the additional case with isotropic grid. For the anisotropic cases, the mean in Figure 9(a) indicates that SGS model has a slight effect. This effect is clarified by the trend of momemtum thickness in Figure 9(b). The momemtum thickness growth is slightly slowed down as the dissipative effect of SGS is increased or equivalently as the eddy viscosity from SGS model is increased (see peak ν_{Tx}/ν for anisotropic cases in Table I). Comparison of the isotropic case (symbol ○) with the anisotropic case (symbol □) indicates that the growth of the momemtum thickness is faster for the isotropic case because of lower eddy viscosity (see peak ν_{Tx}/ν in Table I).

Figures 10(a)–10(b) shows that the peaks and the profiles of rmsu$'/\Delta U$ and rmsv$'/\Delta U$ are lowered as the effect of SGS is increased by increasing eddy viscosity. The quantity rmsω' in

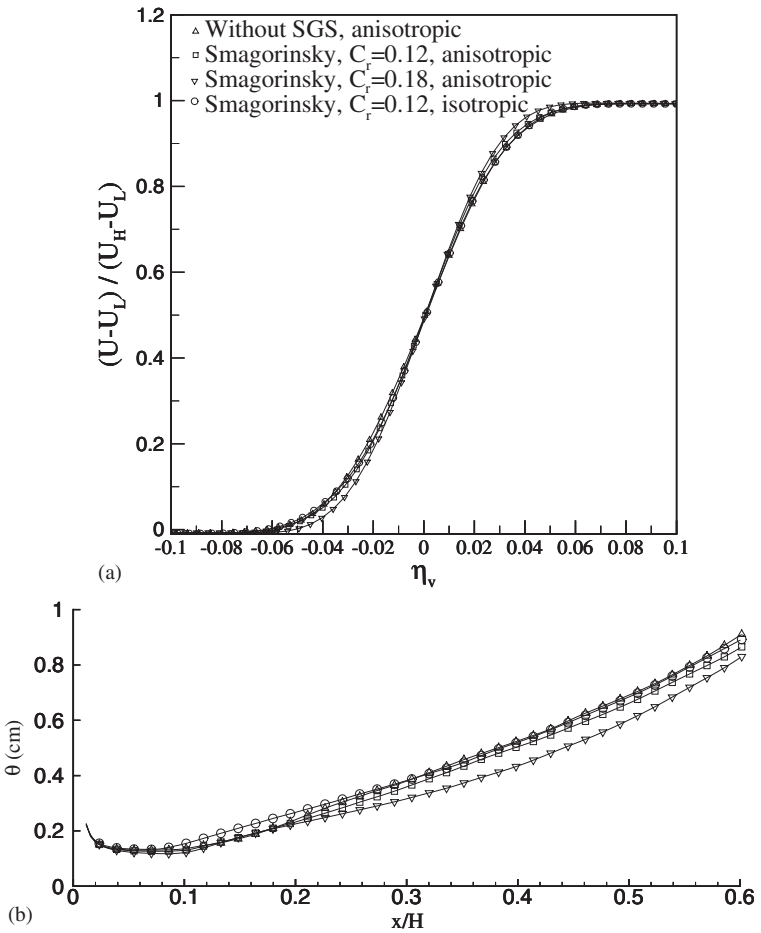

Figure 9. Effect of Subgrid Scale on (a) streamwise mean velocity at $x/H = 0.6$; (b) downstream evolution of momemtum thickness.

Figure 10(d) is lowered as the effect of SGS is increased, consistent with the lower contour level peaks in Figures 7(a)–7(c) and 8(a)–8(c). The Reynolds shear stress $-u'v'/\Delta U^2$ is less affected by SGS, consistent with being linked to the mean in Figure 9(a) by the mean momemtum equation and the mean flow is slightly affected by SGS. Furthermore, Table I shows that the ratio rmsu′/rmsv′ for LES with anisotropic grid is closer to the cases without SGS than the LES with isotropic grid. This is one of the justification for using an anisotropic grid in LES [35]. Furthermore in Figure 10(a), the peak value and the profile trend of the rmsu′/ΔU without SGS agree well with the experimental data of MB at one location $x = 6$ cm as shown in Figure 2(b), whereas the peak value and the profile trend of the rmsu′/ΔU with SGS and $C_r = 0.18$ agree well with the experimental data of MB at three downstream locations $x = 13$, 16 and 19cm as can be inferred by comparing Figure 10(a) with Figure 2(b). However, direct comparison between the unfiltered experimental data of MB and the LES results (filtered results) is unwarranted. Therefore comparison between LES results and experiment of MB

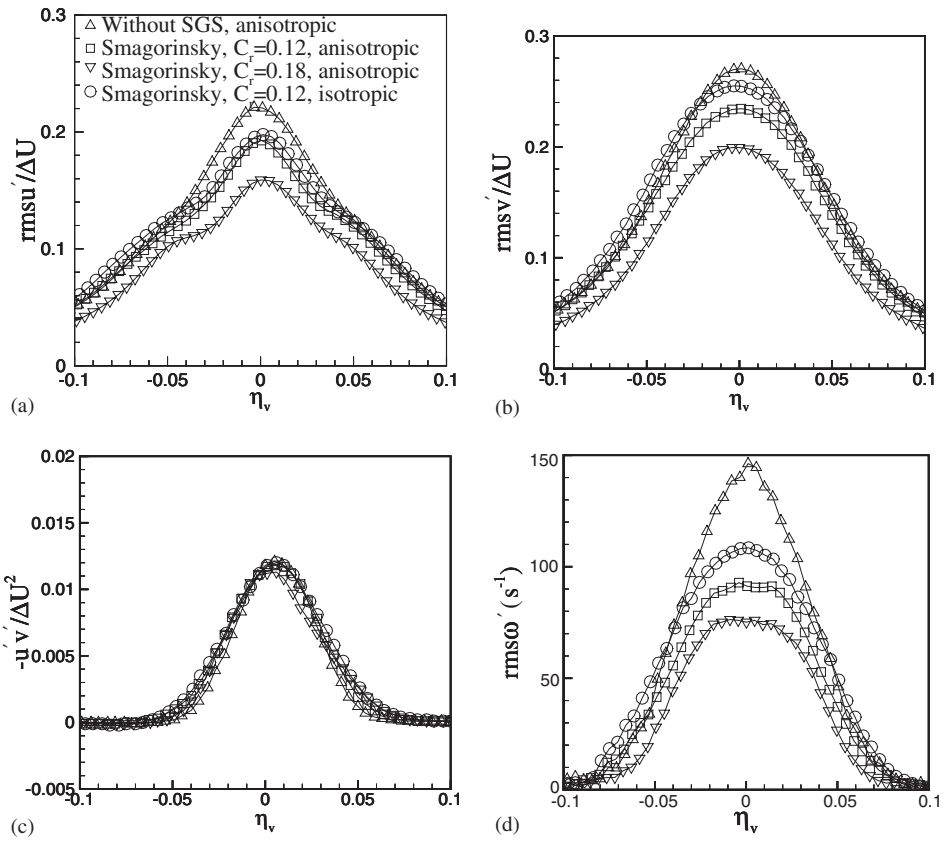

Figure 10. Effect of constant in SGS model and grid on (a) rms longitudinal velocity fluctuations, (b) rms lateral velocity fluctuations, (c) negative cross-stream correlation, (d) rms vorticity fluctuations at $x/H = 0.6$.

Table I. Effect of SGS and grid on instantaneous peak v_{Tx}/v and rmsu′/rmsv′ at $x/H = 0.6$.

C_r	Grid	Peak v_{Tx}/v of last time-step	rmsu′/rmsv′
0 (without SGS)	isotropic (fine)	0	0.817
0 (without SGS)	anisotropic (coarse), △	0	0.817
0.12	anisotropic (coarse), □	18	0.82
0.18	anisotropic (coarse), ▽	58	0.804
0.12	isotropic (fine), ○	6	0.773

has been avoided. It should be noted that the experiment of MB has been chosen in this study because the two-dimensionality of the flow was carefully maintained and verified and also to compare the present results with the simulation [17] who predicted the experiment of MB as discussed in Section 6.2.

7. CONCLUDING REMARKS

An incompressible LES based on the diffusion-velocity method for the vorticity equation and an eddy viscosity SGS model has been developed. In the context of the vortex method, the SGS terms in the vorticity equation produce convection of vortex particles governed by the diffusion-velocity. The two-dimensional vortex-in-cell in conjunction with the Smagorinsky SGS model has been used to calculate the flow field. The technique has been used to calculate the flow characteristics of spatially developing mixing layer. The diffusion-velocity requires one constraint, i.e. nullifying it in regions of small vorticity and non-zero vorticity gradient.

The results by the diffusion-velocity method are in reasonable agreement with those of the random walk, a fundamentally different approach, when the SGS model is not used. The self-similarity of the mean streamwise velocity, rms velocity fluctuations and Reynolds shear stress profiles is consistent with previous numerical simulation when the SGS model is used. The dissipative effect of the SGS model produced by the diffusion-velocity was demonstrated by the slower momemtum thickness development, lower contour values and cross-stream profiles for spanwise vorticity, lower cross-stream profiles for rms longitudinal and lateral velocity fluctuations as the eddy viscosity from SGS model is increased. The effect of anisotropic and isotropic computational grid is in agreement with previous numerical simulations. In future studies, the diffusion-velocity method in conjunction with eddy viscosity based SGS models will be extended to three-dimensional calculations together with DNS calculations.

ACKNOWLEDGEMENTS

This research was supported by a grant from the National Sciences and Engineering Research Council of Canada.

REFERENCES

1. Mansfield JR, Knio OM, Meneveau C. A dynamic LES scheme for the vorticity transport equation: formulation and *a priori* tests. *Journal of Computational Physics* 1988; **145**:693–730.
2. Degond P, Mas-Gallic S. The weighted particle method for convection-diffusion equations. Part 1: the case of isotropic viscosity. *Mathematics of Computation* 1989; **53**(188):485–507.
3. Milane RE, Nourazar, S. On the turbulent diffusion velocity in mixing layer simulated using the vortex method and the subgrid scale vorticity model. *Mechanics Research Communication* 1995; **22**(4):327–333.
4. Milane RE, Nourazar S. Large-eddy simulation of mixing layer using vortex method: effect of subgrid-scale models on early development. *Mechanics Research Communication* 1997; **24**(2):215–221.
5. Mansour NN, Moin P, Reynolds WC, Ferziger JH. Improved method for turbulence. *Turbulence and Shear Flow* I 1979; 386–401.
6. Bardina J, Ferziger JH, Reynolds WC. Improved subgrid models for large eddy simulation. *AIAA* 1980; 1357.
7. Greengard C. The core spreading vortex method approximates the wrong equation. *Journal of Computational Physics* 1985; **61**:345–348.
8. Cottet GH, Koumoutsakos PD. *Vortex Methods*: *Theory and Practice*. Cambridge University 2000.
9. Cottet GH. Artificial viscosity models for vortex and particle methods. *Journal of Computational Physics* 1996; **127**:299–308.
10. Ogami Y, Akamatsu T. Viscous flow simulation using the discrete vortex model—the diffusion velocity method. *Computers and Fluids* 1991; **19**(3/4):433–441.
11. Clarke NR, Tutty OR. Construction and validation of a discrete vortex method for the two-dimensional incompressible Navier–Stokes equations. *Computers and Fluids* 1994; **23**(6):751–783.
12. Ogami Y. A vortex method for heat-vortex interaction and fast summation technique. *First International Conference on Vortex Methods (Kobo)*. World Scientific, Singapore, 1999: **145**:152.
13. Lacombe G, Mas-Gallic S. Presentation and analysis of a diffusion-velocity method. *ESAIM Proceedings* 1999; **7**:225–233.

14. Beaudoin A, Huberson S, Rivoalen E. Simulation of anisotropic diffusion by means of a diffusion velocity method. *Journal of Computational Physics* 2003; **186**:122–135.
15. Abdolhosseini R, Milane RE. On the effect of vortex grid density in the vortex-in-cell simulation of mixing layer. *International Journal of Fluid Dynamics* 2000; **13**:161–183.
16. Inoue O. Double-frequency forcing on spatially growing mixing layers. *Journal of Fluid Mechanics* 1992; **234**:553–581.
17. Ghoneim AF, Heidarinejad G. Effect of two-dimensional shear layer dynamics on mixing and combustion at low heat release. *Combustion Science and Technology* 1990; **72**:79–99.
18. Sarpkaya E. Vortex element methods for flow simulation. *Advances in Applied Mathematics* 1994; **31**: 113–247.
19. Chorin AJ, Marsden JE. *A Mathematical Introduction to Fluid Mechanics*. Springer: Berlin, 1979.
20. Leonard A. Vortex methods for flow simulation. *Journal of Computational Physics* 1980; **37**:289.
21. Ghoneim AF, Givi P. Vortex-scalar element calculations of a diffusion flame stabilized on a plane mixing layer. *NASA Technical Memograph* 100133 ICOMP-87-4 1987.
22. Masutani SM, Bowman CT. The structure of a chemically reacting plane mixing layer. *Journal of Fluid Mechanics* 1986; **172**:93–126.
23. Batchelor GK. *An Introduction to Fluid Dynamics*. Cambridge University Press: Cambridge, 1967.
24. Chorin AJ. Numerical study of slightly viscous flow. *Journal of Fluid Mechanics* 1973; **57**:785–796.
25. Zahrai S, Bark FH, Karlsson RI. On anisotropic subgrid modelling. *European Journal of Mechanics B/Fluids* 1995; **14**(4):459–486.
26. Sagaut P. Large eddy simulation for incompressible flows. *Scientific Computation*. Springer: Berlin, 2002.
27. Vreman B, Geurts B, Kuerten H. Large-eddy simulation of the turbulent mixing layer. *Journal of Fluid Mechanics* 1997; **339**:357–390.
28. Ghoneim AF, Heidarinejad G, Krishnan A. Numerical simulation of a thermally stratified shear layer using the vortex element method. *Journal of Computational Physics* 1988; **79**:135.
29. Baker GR. The cloud-in-cell technique applied to the roll-up of the vortex sheets. *Journal of Computational Physics* 1979; **31**:76–95.
30. Monkewitz PA, Huerre P. Influence of the velocity ratio on the spatial instability of mixing layers. *Physics of Fluids* 1982; **25**:7.
31. Oster D, Wygnanski I. The forced mixing layer between parallel streams. *Journal of Fluid Mechanics* 1982; **123**:91–130.
32. Spencer BW, Jones BG. Statistical investigation of pressure and velocity fields in turbulence two-stream mixing layer. *AIAA 4th Fluid and Plasma Dynamic Conference*, 1971.
33. Deardoff J. A numerical study of three-dimensional turbulent channel flow at large Reynolds numbers. *Journal of Fluid Mechanics* 1970; **41**(2):453–480.
34. Shumann U. Subgrid scale model for finite difference simulations of turbulent flows in plane channels and annuli. *Journal of Computational Physics* 1975; **18**:376–404.
35. Kaltenbach H-J. Cell aspect ratio dependence of anisotropy measures for resolved and subgrid scale stresses. *Journal of Computational Physics* 1997; **136**:399–410.

